





Interplanetary Shock Candidates Observed at Venus's Orbit

Can Wang^{1,2,3} , Mengjiao Xu^{1,2} , Chenglong Shen^{1,2}, Yutian Chi^{1,2,4} , and Yuming Wang^{1,2,5} 

¹ CAS Key Laboratory of Geospace Environment, Department of Geophysics and Planetary Sciences, University of Science and Technology of China, Hefei, Anhui 230026, People's Republic of China; clshen@ustc.edu.cn

² CAS Center for Excellence in Comparative Planetology, University of Science and Technology of China, Hefei, People's Republic of China

³ Institute of Geophysics, China Earthquake Administration, Beijing 100081, People's Republic of China

⁴ Department of Meteorology, University of Reading, Berkshire, UK

⁵ Mengcheng National Geophysical Observatory, School of Earth and Space Sciences, University of Science and Technology of China, Hefei 230026, People's Republic of China

Received 2020 December 19; revised 2021 March 11; accepted 2021 March 12; published 2021 May 7

Abstract

The measurements from the Venus Express spacecraft are analyzed for the basic properties of fast forward interplanetary shocks at Venus's orbit (~ 0.72 au). A total of 143 fast forward interplanetary shock candidates during 2006–2014 are identified. The shock angle Θ_{Bn} , defined as the angle between the shock normal and the upstream magnetic field, and the magnetic compression ratio r_{B} , defined as the ratio of the magnetic field strength downstream to that upstream, of these shocks are determined based on the magnetic coplanarity method. The shock occurrence at Venus shows a correlated variation with the solar activity level measured by the number of sunspots, while the shock angle and magnetic compression ratio do not show such a correspondence. The shock angle spreads almost uniformly between 10° and 80° with its mean value at about 45° , and the magnetic compression ratio shows a unimodal distribution between 1.0 and 4.5 with a mean value of 2.1. In addition, we also analyze the properties of fast forward shocks driven by interplanetary coronal mass ejections (ICMEs). We found that interplanetary shocks with and without detected ICMEs showed no significant differences in terms of the shock strength and the shock angle. Further comparison with previous observational results at 1 au shows that fast forward shocks at 1 au are generally weaker than those at 0.72 au, and the shock angle Θ_{Bn} is more perpendicular at 1 au.

Unified Astronomy Thesaurus concepts: [Venus \(1763\)](#); [Solar system terrestrial planets \(797\)](#); [Interplanetary shocks \(829\)](#)

1. Introduction

Interplanetary (IP) shocks are large-scale perturbations propagating in the heliosphere. They are important as they accelerate charged particles to high energies and generate radio waves and plasma waves, which in turn cause geomagnetic disturbances (e.g., Gonzalez et al. 1999; Echer & Gonzalez 2004; Echer et al. 2008; Huttunen & Koskinen 2004; Kilpua et al. 2017; Shen et al. 2018). The two major drivers of IP shocks are interplanetary coronal mass ejections (ICMEs) and corotating interaction regions (CIRs). ICMEs are the primary drivers of IP shocks within 1 au (Berdichevsky et al. 2000; Echer et al. 2005; Oh et al. 2007; Kilpua et al. 2015), while CIR shocks typically develop in the solar wind beyond 2 au (Gosling et al. 1976; Smith & Wolfe 1976).

Fast forward IP shocks are the most frequently observed shocks in the IP space. In the literature, shock characteristics are commonly defined by their strength and geometry. The Mach number (M_{a}) and the compression ratio (r) are used as indicators of the shock strength. The angle (θ_{Bn}) between the shock normal and the upstream magnetic field describes the geometry of IP shocks, which influences the mechanism of particle acceleration at the shock (Reames 1999). These parameters may change significantly for each shock and for different heliocentric distances. Using in situ observations, the local parameters of IP shocks could be estimated by different methods, including the magnetic coplanarity method (Colburn & Sonett 1966), the velocity coplanarity method (Abraham-Shrauner & Yun 1976), the mixed-mode method (Abraham-Shrauner 1972; Abraham-Shrauner & Yun 1976), and the

Rankine–Hugoniot method (Viñas & Scudder 1986). All these methods assume the Rankine–Hugoniot relationship which accounts for momentum and energy conservation across the shock surface, but use different subsets of solar wind and interplanetary magnetic field (IMF) data.

IP shocks have been extensively studied near 1 au. A number of studies have considered their statistically averaged properties (Tsurutani & Lin 1985; Bavassano-Cattaneo et al. 1986; Echer et al. 2003; Lario et al. 2005; Oh et al. 2007; Neugebauer 2013; Kilpua et al. 2015; Oliveira & Raeder 2015). In general, IP shocks detected near the Earth's orbit are on average slow and weak. Some researchers have found that the majority of IP shocks have a compression ratio between 1.2 and 2.0, with a mean Mach number of 2.1 (Tsurutani & Lin 1985; Berdichevsky et al. 2000; Kilpua et al. 2015; Oliveira & Raeder 2015). Oliveira & Raeder (2015) reported that the speed of most IP shocks exceeds 400 km s^{-1} , with an average speed of 467 km s^{-1} , by studying 451 fast forward IP shocks observed by Wind and the Advanced Composition Explorer (ACE). In addition, IP shocks are more likely to be quasi-perpendicular ($\theta_{\text{Bn}} > 45^\circ$). At 1 au, the frequencies of IP shocks per year follow the variation of solar activities (Berdichevsky et al. 2000; Echer et al. 2003; Oh et al. 2007; Kilpua et al. 2015; Oliveira & Raeder 2015). IP shocks are typically faster during solar maxima than during solar minima, while the shock compression ratio and the Mach number do not clearly follow the solar cycle variations (Echer et al. 2003; Oh et al. 2007; Kilpua et al. 2015).

IP shock studies near Venus have been done principally with the Pioneer Venus Orbiter (PVO) mission (Mihalov 1985;

Mihalov et al. 1987; Lindsay et al. 1994; Jian et al. 2008). Using data from PVO, Lindsay et al. (1994) found that most of the shocks at 0.72 au are associated with ICMs. Mihalov et al. (1987) compared shock parameters obtained from PVO observations with the published results near Earth, finding that the shock strength decreases with distance and the shock speed decelerates as they propagate away from the Sun. The launch of Venus Express (VEX; Titov et al. 2006; Svedhem et al. 2007) provides a new opportunity to study IP magnetic structures near Venus, allowing the study of more IP shocks at 0.72 au. Compared with PVO observations, VEX was launched with improved instrument capability, such as a much higher resolution and sampling rate for its magnetometer and plasma analyzer (Zhang et al. 2006). Using VEX observations, the structure of the Venusian magnetosphere has been investigated by some researchers (Zhang et al. 2008, 2009, 2010; Chai et al. 2014; Shan et al. 2015; Vech et al. 2016; Xiao et al. 2020). The magnetic barrier was found at lower altitudes during the solar minimum than that during the solar maximum (Zhang et al. 2008), and it also showed an IMF dependence (Zhang et al. 2009; Vech et al. 2016). Shan et al. (2015) reported that the location of Venus's bow shock is further out at the solar maximum; the terminator shock distance at the solar minimum is equivalent to that determined by PVO. Based on the magnetic field data from VEX observed down to 130 km altitude, Zhang et al. (2016) reported weaker and quieter magnetic field variations below the ionosphere. The VEX measurements with a higher resolution and sampling rate can further refine our understanding of the formation, structure, and properties of IP shocks.

The main goal of this paper is to establish a list of possible fast forward IP shocks near Venus's orbit (~ 0.72 au), and to investigate their shock properties. Using VEX 1 s magnetic field data during the whole period of VEX's observation, fast forward IP shocks are identified and shock parameters are determined. However, we cannot rule out the possibility that we have counted other discontinuities or slow reverse shocks as fast forward IP shocks given the lack of plasma data; all the events in our list should therefore be considered as IP shock candidates. Based on the obtained parameters, we present a statistical analysis to investigate the characteristics of IP shocks at 0.72 au and their solar cycle variation. Furthermore, we also analyze shock properties of IP shocks driven by ICMs. Based on the statistical results obtained in this study, we are able to confirm some earlier results and compare characteristics of IP shocks at 0.72 au and at 1 au.

2. Used Data and Methods

2.1. Data Sets

The magnetic field data used to identify shocks was recorded by the magnetometer on board the VEX spacecraft. VEX was a European Space Agency mission injected into Venus's orbit in 2006 April and terminated in 2014 December (Titov et al. 2006; Svedhem et al. 2007). VEX carried a fluxgate magnetometer which observed the magnetic field continuously with a 1 Hz sampling rate in Venus solar orbital (VSO) coordinates, in which X points from Venus toward the Sun, Y points from Venus in the opposite direction of the planet's orbital motion, and Z completes the right-handed system (Zhang et al. 2006). Although the VEX payload included a plasma analyzer (the Analyzer of Space Plasmas and Energetic

Atoms version 4; Barabash et al. 2007), it was operated only close to Venus, starting and ending just outside the Venus bow shock, so there are no plasma data available for studying the structure of the solar wind such as IP shocks.

Without an intrinsic magnetic field, Venus interacts with the solar wind directly on its upper ionosphere and forms an induced magnetosphere (Luhmann 1986). Based on the PVO mission, it has been found that the average location of the bow shock is 2.40 Venus radii (Rv, 6051.8 km) at the solar maximum and 2.14 Rv at the solar minimum, which changes with solar activity (Russell et al. 1988). This results in perturbation in the magnetic field observations when VEX moved in and out Venus's magnetosphere. In order to obtain a solar-wind-only data set for shock analysis, the magnetosphere measurements were cleaned by removing VEX data inside of 3.0 Rv. We use a larger shock terminator distance of 3.0 Rv instead of the average bow shock position of 2.40 and 2.14 Rv (Russell et al. 1988), which can remove almost all the induced magnetospheric passes while still keeping vast amounts of solar wind data.

2.2. Shock Analysis Method

A simple two-step shock detection routine was applied to identify fast forward IP shocks. We first used an auto-search program to identify potential IP shocks in the entire available VEX data set, then visually inspected each event.

Fast forward IP shocks are observed as a sudden steplike increase in solar wind plasma parameters and the magnetic field strength. Since plasma data are not available for VEX, shocks are identified by their magnetic field signatures alone in this work. For the initial automated finding of a suitable shock candidate, each of two consecutive data points were compared to look for discontinuous change in the magnetic field magnitude. Two criteria were used to identify shocks in magnetic field data: (1) that the presence of a magnetic field jump occurred in at least one magnetic field component; (2) the magnetic field magnitude jump ratio should be no less than 1.3. By satisfying these two conditions, the event will be counted as a shock candidate. In this step, we identified 982 fast forward IP shock candidates that satisfied the mentioned criteria.

To improve the shock-finding result, the averages of magnetic field data were used as the next shock test. The short time magnetic fluctuations or other solar wind discontinuities can lead to false IP shock detection, since they can reach a magnitude similar to the shock, and happen as suddenly as shock occurred, but appear on a shorter timescale. Thus an examination of 20 minutes data either side of the discontinuity was performed to avoid false shock detection. These data were averaged in the upstream and downstream for every 5 minutes. In this way we obtained four averaged values on either side of the discontinuity, each 5 minute mean upstream and downstream pair were compared and had the same shock identification conditions applied as above. The purpose of this examination is to discriminate against short time fluctuations of the magnetic field. This step reduces the number of fast forward IP shock candidates from 982 to 234.

The above auto-search method is flexible and may identify as many IP shocks as possible, though still with, however, a few false shock detections. Finally, every shock candidate was visually inspected in high-resolution magnetic field plots to confirm discontinuities as a shock. This inspection ensures that we have discarded all the fluctuations and other solar wind

discontinuities. We identified a total of 143 fast forward IP shocks near VEX’s orbit between 2006 April and 2014 November.

Once a shock was identified, their shock parameters were calculated. The shock normal analyses were performed using the magnetic coplanarity theorem (Colburn & Sonett 1966), since it only requires magnetic field data. The shock normal (\hat{n}) is related to the upstream (B_u) and downstream (B_d) magnetic field by

$$\hat{n} = \pm \frac{(B_u \times B_d) \times (B_u - B_d)}{|(B_u \times B_d) \times (B_u - B_d)|}.$$

In this study, B_u and B_d are the averaged upstream and downstream magnetic field vectors, which were determined in 10 minute time intervals on either side of the shock in order to calculate their local shock parameters. The upstream and downstream intervals were carefully chosen to ensure that the selected high-resolution magnetic field data were relatively steady. If the magnetic field observations before or after the shock were contaminated by an unrelated event, the time period was shortened to remove large fluctuations. The shock parameters calculated in this work were the shock angle Θ_{Bn} , the angle between the shock normal and the upstream magnetic field, and the magnetic compression ratio r_B , which is defined as the ratio of the magnetic field strength in the downstream to that in the upstream. Depending on the value of Θ_{Bn} , an IP shock can be classified as a quasi-perpendicular shock when $\Theta_{Bn} > 45^\circ$, and a quasi-parallel shock when $\Theta_{Bn} \leq 45^\circ$ (Fairfield 1976; Omid 1995).

The list of fast forward IP shocks and their shock parameters are shown in Table 1. The columns are event number, shock arrival date and time at the spacecraft, shock normal directions, shock angle (Θ_{Bn}), shock magnetic compression ratio (r_B), and the last column indicates IP shocks associated with a detected ICME by “CME.” Figure 1 shows a fast forward IP shock in VEX magnetic field observations on 2011 September 9, displayed in VSO coordinates. The shock is indicated by the letter “S” and vertical dashed lines. The upstream and downstream intervals are marked by horizontal lines and the letters “U” and “D” respectively. The shock parameters were estimated in these time intervals. This shock was quasi-perpendicular ($\Theta_{Bn} = 49^\circ$), with a magnetic compression ratio of 1.65.

It should be noted that identifying fast forward IP shocks by magnetic field signatures alone is somewhat difficult and ambiguous. Ideally, both magnetic field and solar wind plasma data would be used to identify shocks. In the absence of plasma data from VEX, one issue is differentiating between IP shocks and other solar wind structures such as other discontinuities, as they have similar magnetic signatures. Thus we used the magnetic compression ratio (≥ 1.3) as the primary criterion, which may be useful for distinguishing IP shocks from other discontinuities (Oliveira & Samsonov 2018). To confirm that our shocks are identified correctly, we further verified these events by a pair of radially aligned spacecraft observations. For each shock observed by VEX, the measurements made by spacecraft at 1 au such as Wind or the Solar Terrestrial Relations Observatory (STEREO) have been examined for signatures of the same event.

As the probability and reliability of observing the same shock is higher for smaller spacecraft separations, we searched for conjunction events observed by spacecraft at 1 au and VEX

with their longitudinal separations of less than 10° ; 26 shocks were observed at VEX, 12 of them were also identified as fast forward IP shocks near 1 au. Figure 2 shows a fast forward IP shock that was observed by VEX at 0.72 au and subsequently by STEREO-A at 0.95 au. The eight panels show magnetic field data at VEX and STEREO-A in VSO coordinates (first four from top) and plasma measurements at STEREO-A (bottom four). As shown in Figures 2(a) and (b), a shock arrived at VEX at 20:48:00 UT on 2011 March 18, followed by the sheath region and the magnetic cloud. Approximately 15 hr later, the shock and the driving ICME were also observed at STEREO-A where we have plasma measurements. We can see that both spacecraft observed similar profiles where the magnetic field strength enhanced sharply and the field rotated relatively smoothly, which suggest both spacecraft observed the same shock front. The plasma properties of the shock at STEREO-A show a clear increase in proton bulk speed and proton number density, indicating the shock would most likely have shown a similar plasma signature if plasma data were available at VEX. For all 12 events which were observed by both spacecraft, we visually inspected their magnetic field data at VEX and both plasma and magnetic field data at 1 au. We found that all the shocks observed by both spacecraft were driven by ICMEs, that clear ICME signatures (Zurbuchen & Richardson 2006) detected at both spacecraft, and that observations matched well in magnetic field data at two locations. Besides, they are generally stronger than those shocks that were not detected near 1 au. We believe those shocks observed at two radially aligned spacecraft are true fast forward IP shocks.

Meanwhile, no associated shocks (fast forward or slow reverse shocks) were detected at 1 au for 10 events. Another four shocks were not considered due to the data gap of 1 au observations. Figure 3 shows a shock observed at 15:39:29 UT on 2013 January 13 by VEX, but no observable shock is detected by STEREO-A, although VEX and STEREO-A were only separated by 8° . By analyzing 395 ICME-driven shocks detected by a pair of spacecraft during 1974–1986, de Lucas et al. (2011) also found that for small longitudinal separations between two spacecraft, there were many IP shocks that were observed by only one spacecraft. There are several possible explanations why these potential fast forward IP shocks were not observed near 1 au. One possible reason is that there are other solar structures that are not shocks. Another possibility is that shocks weaken and dissipate during their propagation in the IP space. Note that, however, we cannot be sure that all the events in our list are fast forward IP shocks; these events contain true fast forward IP shocks, and may also contain different discontinuities or slow reverse shocks. The event in our list should therefore be considered as an IP shock candidate. In the following statistical analysis, the “shocks” should be considered as “shock candidates.”

3. Statistical Results

In this section we present a statistical analysis of the occurrence rate and the characteristics of IP shocks; the statistics include 143 fast forward IP shocks listed in Table 1, covering the period from late declining phase of Solar Cycle 23 (SC23) to solar maximum of Solar Cycle 24 (SC24). First, we analyze how the occurrence rate and parameters of IP shocks are related to the solar cycle. Second, we consider the distribution of fast forward IP shock properties at 0.72 au.

Table 1
List of Interplanetary Shocks Identified near 0.72 au by VEX (2006–2014)

Event Number	Date	Time	Shock Normal	θ_{Bn} (deg)	r_B	Type
1	2006-05-30	05:34:30	(−0.19, 0.86, −0.48)	26	1.80	...
2	2006-07-17	04:25:32	(−0.28, 0.95, 0.15)	47	2.27	CME
3	2006-09-10	14:10:46	(−0.95, −0.12, 0.28)	34	3.25	CME
4	2006-11-28	00:58:01	(−0.33, −0.78, −0.54)	49	2.77	...
5	2006-12-06	21:58:32	(−0.35, 0.91, 0.24)	40	2.15	...
6	2007-01-03	17:09:33	(−0.52, −0.83, 0.19)	77	3.84	...
7	2007-01-27	01:30:52	(−0.26, 0.71, 0.66)	79	2.00	...
8	2007-02-22	13:09:50	(−0.17, 0.22, −0.96)	70	2.10	...
9	2007-03-23	23:30:08	(−0.05, 0.93, −0.36)	20	3.77	...
10	2007-04-29	23:50:54	(−0.40, 0.40, 0.83)	52	1.83	...
11	2007-06-25	01:24:58	(−0.44, −0.60, −0.67)	70	3.47	...
12	2007-10-02	13:21:50	(−0.02, −0.76, 0.65)	66	1.72	...
13	2007-11-10	03:55:20	(−0.75, −0.37, 0.55)	13	2.53	...
14	2007-12-21	13:51:50	(−0.68, −0.03, 0.74)	56	1.47	...
15	2008-01-08	14:18:25	(−0.89, 0.44, 0.08)	30	2.08	...
16	2008-01-19	15:01:11	(−0.74, −0.32, −0.59)	82	3.38	...
17	2008-03-30	15:01:07	(−0.24, 0.97, −0.07)	27	1.39	...
18	2008-05-22	15:44:41	(−0.17, 0.85, −0.50)	41	2.02	...
19	2008-06-24	08:55:17	(−0.29, 0.48, 0.83)	30	2.41	CME
20	2008-06-28	10:20:45	(−0.32, 0.86, −0.39)	29	1.64	...
21	2008-09-01	14:16:01	(−0.86, −0.15, 0.48)	52	1.54	...
22	2008-09-18	10:38:18	(−0.36, −0.73, −0.58)	40	2.45	...
23	2008-11-15	23:19:38	(−0.62, −0.78, 0.06)	24	2.86	...
24	2009-01-20	10:30:52	(−0.82, 0.41, 0.40)	35	1.56	...
25	2009-04-28	21:39:28	(−0.87, 0.06, 0.49)	75	1.68	CME
26	2009-05-04	12:10:33	(−0.15, 0.96, −0.24)	47	1.79	...
27	2009-06-06	04:55:30	(−0.44, 0.70, −0.56)	55	1.88	CME
28	2009-09-05	09:50:53	(−0.08, 0.97, 0.22)	35	2.00	CME
29	2009-10-02	15:51:12	(−0.48, −0.26, −0.84)	28	1.75	...
30	2009-10-18	10:02:42	(−0.83, 0.05, −0.56)	84	2.33	...
31	2009-11-03	10:42:34	(−0.97, −0.22, −0.05)	29	1.38	...
32	2009-11-11	12:51:10	(−0.22, 0.53, −0.82)	20	1.98	CME
33	2009-11-15	19:34:28	(−0.33, −0.94, −0.07)	40	1.88	CME
34	2010-02-21	21:06:06	(−0.94, 0.05, −0.34)	66	1.75	...
35	2010-02-23	21:39:18	(−0.12, 0.79, −0.60)	32	1.50	...
36	2010-02-23	22:30:46	(−0.39, 0.68, −0.62)	50	1.61	...
37	2010-02-24	17:01:05	(−0.53, −0.41, −0.74)	54	1.84	...
38	2010-03-03	04:39:37	(−0.35, −0.01, −0.94)	20	2.43	CME
39	2010-03-16	19:11:22	(−0.42, 0.50, −0.76)	29	2.20	CME
40	2010-05-01	01:17:35	(−0.80, −0.56, 0.21)	77	4.39	...
41	2010-06-06	13:39:10	(−0.59, −0.70, −0.4)	50	1.86	CME
42	2010-06-30	17:47:14	(−0.09, −0.50, −0.86)	69	2.00	...
43	2010-08-01	14:41:15	(−0.45, 0.75, −0.48)	56	2.43	CME
44	2010-08-02	11:29:31	(−0.95, 0.31, 0.08)	53	2.66	CME
45	2010-08-05	20:05:55	(−0.78, 0.43, −0.45)	54	1.46	...
46	2010-08-10	03:48:19	(−0.61, 0.44, −0.66)	67	2.86	CME
47	2010-09-10	16:07:23	(−0.30, −0.74, −0.60)	39	1.63	CME
48	2010-09-13	18:59:38	(−0.31, 0.41, 0.86)	58	2.14	...
49	2010-10-01	14:54:24	(−0.35, −0.22, 0.91)	15	2.21	...
50	2010-10-03	13:16:27	(−0.37, −0.22, −0.90)	78	2.01	...
51	2010-10-09	05:51:56	(−0.97, 0.07, 0.24)	55	2.08	...
52	2010-11-09	10:50:50	(−0.39, 0.91, 0.17)	36	1.85	...
53	2010-12-14	07:29:41	(−0.48, −0.75, 0.46)	26	1.77	...
54	2010-12-25	05:53:57	(−0.30, 0.91, 0.29)	56	1.67	...
55	2010-12-25	22:02:25	(−0.90, 0.29, −0.33)	12	2.98	...
56	2011-01-19	21:17:21	(−0.55, −0.68, −0.48)	31	2.41	CME
57	2011-03-08	21:17:29	(−0.78, −0.39, −0.49)	54	2.50	CME
58	2011-03-10	18:29:41	(−0.39, −0.30, −0.87)	17	2.52	CME
59	2011-03-18	20:48:00	(−0.94, 0.12, −0.31)	24	1.69	CME
60	2011-03-21	09:20:04	(−0.94, −0.16, 0.31)	48	1.73	CME
61	2011-03-22	08:51:59	(−0.37, −0.90, 0.22)	72	2.42	CME
62	2011-03-28	07:59:26	(−0.71, 0.52, −0.48)	28	1.43	...
63	2011-04-11	00:35:21	(−0.63, 0.44, −0.64)	24	2.22	CME
64	2011-04-11	07:30:32	(−0.67, 0.62, 0.40)	17	1.59	CME

Table 1
(Continued)

Event Number	Date	Time	Shock Normal	θ_{Bn} (deg)	r_B	Type
65	2011-04-15	21:17:33	(-0.55, 0.73, -0.40)	23	1.95	...
66	2011-05-19	20:58:55	(-0.97, -0.05, -0.26)	41	1.72	CME
67	2011-06-05	05:26:13	(-0.56, -0.77, -0.30)	75	2.09	CME
68	2011-07-27	19:33:10	(-0.96, -0.24, -0.13)	77	2.74	...
69	2011-09-09	01:09:41	(-0.80, 0.60, 0.02)	49	1.65	...
70	2011-09-09	19:19:17	(-0.47, 0.85, 0.25)	37	1.80	...
71	2011-10-03	10:52:42	(-0.91, 0.09, -0.40)	46	1.76	...
72	2011-10-10	08:31:44	(-0.12, -0.06, -0.99)	70	3.08	...
73	2011-10-15	13:04:29	(-0.42, 0.01, -0.91)	37	1.61	...
74	2011-10-16	00:50:52	(-0.04, 0.81, 0.59)	76	2.36	CME
75	2011-11-05	03:41:51	(-0.24, 0.36, 0.90)	14	2.04	CME
76	2011-11-09	11:28:10	(-0.39, 0.89, -0.23)	11	3.17	...
77	2011-12-01	15:48:04	(-0.62, 0.35, -0.70)	15	2.41	CME
78	2011-12-09	17:28:46	(-0.06, -0.95, 0.31)	49	1.46	...
79	2011-12-25	12:38:25	(-0.35, 0.06, -0.94)	55	3.44	CME
80	2012-01-14	22:48:04	(-0.83, 0.31, 0.46)	27	2.04	...
81	2012-01-16	22:20:55	(-0.82, 0.54, -0.20)	64	1.55	CME
82	2012-01-17	23:52:59	(-0.96, 0.27, -0.07)	58	1.80	...
83	2012-01-21	14:24:42	(-0.50, 0.76, -0.42)	66	2.02	...
84	2012-02-11	16:51:09	(-0.44, 0.72, -0.54)	47	2.21	CME
85	2012-02-26	19:05:57	(-0.77, -0.59, -0.25)	26	2.17	...
86	2012-03-05	18:31:46	(-0.20, 0.17, -0.96)	69	2.05	...
87	2012-03-07	13:26:36	(-0.88, 0.30, 0.37)	74	3.68	CME
88	2012-04-25	11:29:12	(-0.33, 0.75, -0.57)	58	1.91	...
89	2012-05-11	21:15:24	(-0.69, 0.71, -0.09)	10	2.21	CME
90	2012-06-15	08:30:12	(-0.53, -0.65, -0.54)	29	1.94	CME
91	2012-06-16	04:53:36	(-0.92, 0.02, 0.38)	83	2.02	CME
92	2012-07-10	18:59:51	(-0.96, -0.21, -0.16)	64	1.57	...
93	2012-07-15	14:25:18	(-0.77, -0.64, -0.02)	20	2.81	...
94	2012-07-18	16:38:29	(-0.32, -0.53, 0.79)	59	2.72	CME
95	2012-07-20	09:15:04	(-0.31, 0.13, 0.94)	21	2.08	...
96	2012-07-29	05:28:09	(-0.73, -0.65, 0.22)	35	1.61	CME
97	2012-08-25	20:38:12	(-0.94, 0.21, 0.27)	67	1.73	...
98	2012-09-03	09:20:09	(-0.77, 0.28, 0.57)	81	1.57	...
99	2012-09-13	04:44:17	(-0.68, 0.50, 0.53)	51	2.36	CME
100	2012-09-30	06:14:07	(-0.52, -0.73, -0.44)	49	2.44	...
101	2012-11-10	15:39:08	(-0.94, 0.33, 0.12)	11	2.05	CME
102	2012-11-13	10:47:22	(-0.76, 0.37, -0.53)	78	1.98	CME
103	2012-11-25	12:55:01	(-0.82, -0.18, 0.55)	60	1.42	...
104	2012-12-09	18:50:03	(-0.85, 0.21, -0.49)	19	2.03	...
105	2013-01-08	09:22:25	(-0.81, -0.28, 0.52)	58	2.69	CME
106	2013-01-13	15:39:29	(-0.19, -0.95, 0.25)	38	1.96	...
107	2013-02-11	20:45:26	(-0.78, 0.16, 0.60)	37	1.65	...
108	2013-02-21	13:11:58	(-0.07, 0.33, -0.94)	19	1.55	CME
109	2013-02-28	12:17:18	(-1.00, 0.06, -0.02)	70	1.84	...
110	2013-03-06	13:22:08	(-0.86, -0.47, 0.20)	68	2.76	CME
111	2013-04-27	14:37:59	(-0.79, 0.57, -0.23)	6	1.93	CME
112	2013-05-01	09:56:45	(-0.61, -0.77, 0.19)	80	1.62	...
113	2013-05-11	20:49:55	(-0.13, 0.37, 0.92)	26	1.70	...
114	2013-05-13	10:11:39	(-0.69, -0.55, 0.48)	66	1.54	...
115	2013-05-14	19:51:05	(-0.82, 0.45, 0.36)	21	1.98	CME
116	2013-06-01	08:18:07	(-0.68, -0.64, 0.37)	74	2.01	CME
117	2013-07-02	18:59:45	(-0.74, 0.22, -0.63)	18	1.30	...
118	2013-07-20	10:05:33	(-0.46, 0.77, -0.44)	64	2.01	CME
119	2013-09-01	04:06:33	(-0.98, -0.18, -0.05)	11	1.56	...
120	2013-10-05	04:17:24	(-0.77, -0.61, -0.18)	70	1.86	CME
121	2013-10-22	22:40:57	(-0.04, -0.97, -0.23)	48	1.60	...
122	2013-10-27	11:13:52	(-0.43, 0.69, 0.57)	51	3.08	CME
123	2013-10-30	17:20:11	(-0.72, -0.49, 0.49)	5	2.18	...
124	2013-11-25	05:54:18	(-0.66, 0.15, -0.74)	20	1.50	...
125	2013-11-30	04:30:13	(-0.85, 0.19, 0.48)	57	2.91	CME
126	2013-12-14	03:06:35	(-0.96, 0.15, 0.25)	69	2.63	CME
127	2013-12-23	19:08:58	(-0.06, -0.95, -0.31)	59	1.65	...
128	2014-02-19	21:25:34	(-0.18, -0.92, -0.34)	60	2.16	CME

Table 1
(Continued)

Event Number	Date	Time	Shock Normal	θ_{Bn} (deg)	r_B	Type
129	2014-02-24	21:18:19	(−0.04, 0.83, 0.56)	11	2.10	...
130	2014-03-31	17:42:03	(−0.87, 0.28, 0.40)	34	1.42	CME
131	2014-04-20	06:56:04	(−0.40, −0.68, −0.61)	79	2.68	CME
132	2014-05-05	12:26:14	(−0.07, 0.78, 0.62)	37	2.21	...
133	2014-05-10	18:05:36	(−0.86, 0.17, 0.48)	65	1.61	...
134	2014-06-10	05:12:44	(−0.56, −0.58, −0.59)	80	2.27	CME
135	2014-06-15	06:56:19	(−0.59, 0.61, 0.52)	21	2.29	...
136	2014-06-18	09:24:56	(−0.85, 0.26, 0.47)	32	1.64	...
137	2014-07-29	09:00:18	(−0.41, 0.05, −0.91)	11	2.08	CME
138	2014-08-31	07:10:20	(−0.14, −0.49, 0.86)	19	2.02	...
139	2014-09-02	00:31:55	(−0.69, −0.69, −0.22)	23	1.39	...
140	2014-09-23	18:56:04	(−0.66, 0.56, 0.51)	48	1.77	CME
141	2014-09-25	05:02:47	(−0.38, 0.50, −0.78)	86	1.62	...
142	2014-09-26	05:29:14	(−0.07, −0.78, −0.62)	40	2.20	...
143	2014-09-26	13:35:34	(−0.55, −0.02, 0.83)	36	1.69	CME

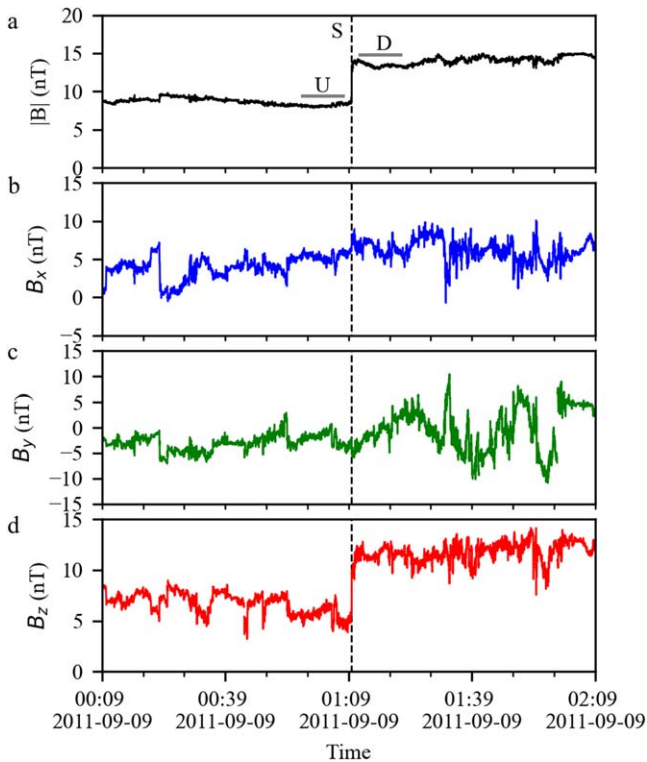


Figure 1. Example of a fast forward IP shock detected by VEX on 2011 September 9. From top to bottom are (a) total magnetic field, and (b)–(d) magnetic field components B_x , B_y , B_z in VSO coordinates. The shock is indicated by the letter “S” and the vertical dashed line. The upstream and downstream intervals are marked by horizontal lines and letters “U” and “D,” respectively.

Finally, we discuss the properties of fast forward shocks driven by a detected ICME.

3.1. Solar Cycle Variations of Shock Rate and Shock Properties

The yearly number of near-Venus IP shocks is shown in Figure 4(a); the blue bar shows the number of IP shocks identified in the VEX data, while the solid black line represents the solar activity level indicated by the yearly mean sunspot number. It can be seen in Figure 4 that the number of sunspots

reached a minimum value around the year 2008, which is the end of SC23, and peaked in 2014, the solar maximum of SC24. We can find that the annual IP shock numbers roughly follow the changes in the number of sunspots. Few IP shocks occurred around the solar minimum (nine shocks observed in 2008), while the number of shocks showed a remarkable increase as the solar activity intensified. The annual occurrence of IP shocks peaked in 2012 with the highest value of 25 IP shocks per year, but decreased in 2014. Similar trends were also observed at 1 au by Oliveira & Samsonov (2018), who reported that the IP shock number during the ascending phase of SC24 was larger than during the maximum phase of SC24 (2014). The correlation coefficient between the yearly occurrence frequencies of IP shocks and the sunspot numbers is 0.69, which showed a moderate correlation. It should be pointed out that the clear dip in the shock frequencies in 2006 and 2014 perhaps relates to the gaps in magnetic field data; the fractions of available data are only 61% in the mission-beginning year (2006) and 70% in the mission-ending year (2014). Without using data for 2006 and 2014, the correlation coefficient increases to 0.87, which is slightly higher than the correlation coefficient (>0.7) obtained at 1 au (Wu & Lepping 2016). In general, the occurrence of IP shocks at 0.72 au is associated with the number of sunspots, which is in accordance with the early study obtained by Lindsay et al. (1994). Lindsay et al. (1994) analyzed 45 IP shocks observed by PVO during the period of 1979–1988, suggesting a solar cycle dependence of IP shocks at 0.72 au. Many authors also reported that the annual rate of IP shocks at 1 au correlates well with the number of sunspots (Berdichevsky et al. 2000; Echer et al. 2003; Oh et al. 2007; Kilpua et al. 2015; Oliveira & Raeder 2015).

The bottom two panels of Figure 4 show the annual mean of shock parameters with respect to the time. The yearly averaged shock angle Θ_{Bn} displays random variations during the investigated period, without any relationship to solar activities. We also calculated the ratio of quasi-perpendicular shocks to quasi-parallel shocks in each year, and it varies randomly without any solar cycle trend. The shock strength, which is characterized by the annual mean of the magnetic compression ratio r_B here, does not show a clear solar cycle variation either. It appears to be slightly stronger in the late declining phase of SC23 than in the solar maximum of SC24. Similar to our present study, Echer et al. (2003) and Kilpua et al. (2015)

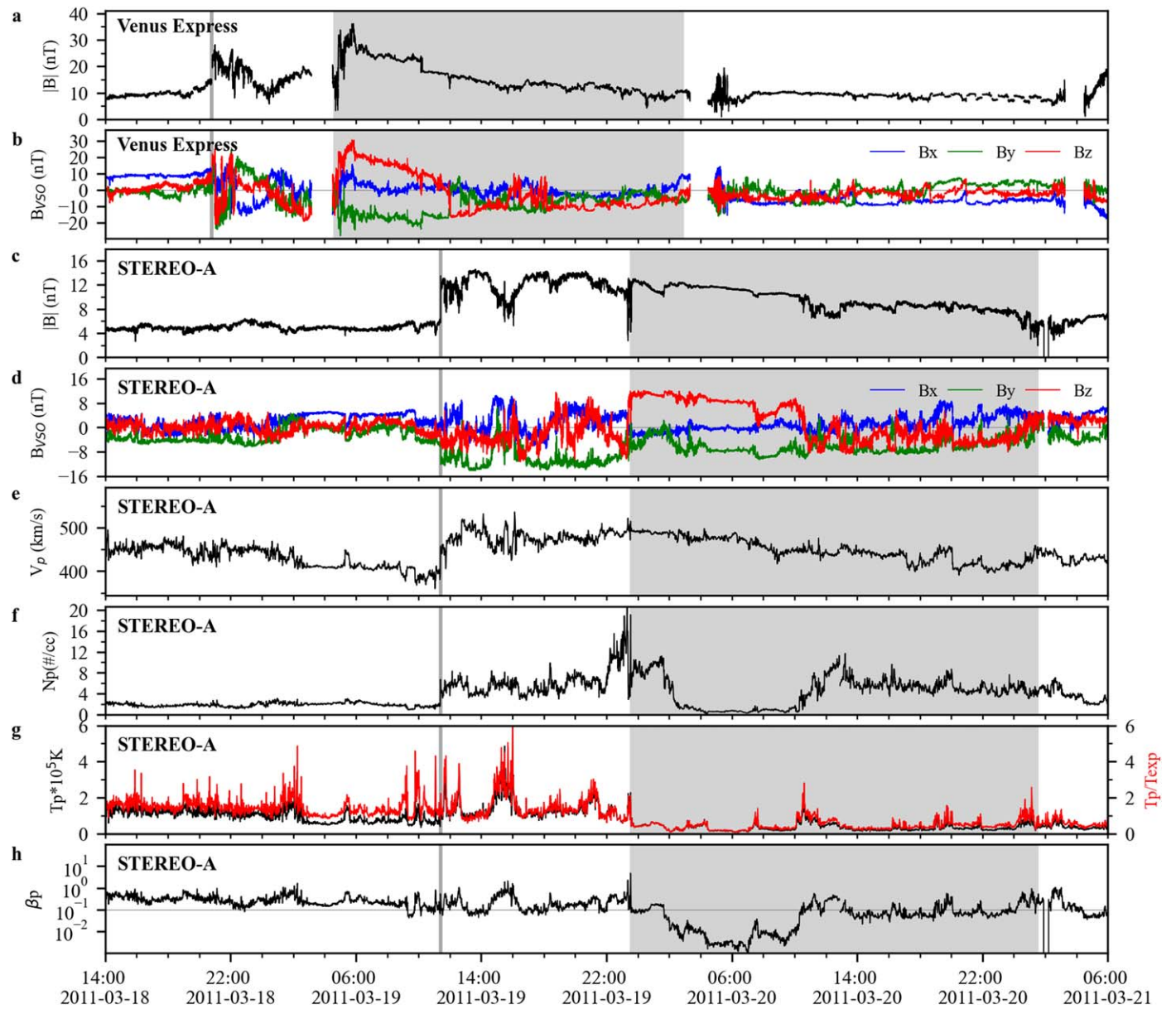


Figure 2. Fast forward IP shock measurements at VEX and STEREO-A. The panels from top to bottom represent: (a) the magnetic field strength at VEX; (b) B_x , B_y , B_z magnetic field components at VEX in VSO coordinates; (c) the magnetic field strength at STEREO-A; (d) B_x , B_y , B_z magnetic field components at STEREO-A in VSO coordinates; (e)–(h) the proton bulk speed, the proton density, temperature (red solid line, expected temperature from Lopez 1987), and proton β at STEREO-A. The vertical gray line marks the shock arrival, and the shaded region indicates the ICME interval.

concluded that at 1 au, the shock angle and the shock strength do not show any relationship to the solar cycle.

3.2. Distribution of Shock Parameters

Figure 5 shows histograms of the shock angle and magnetic compression ratio for all shocks observed at 0.72 au. The vertical lines give the mean and median values of shock parameters in each panel of Figure 5.

The shocks in our list show a very large spread of shock angle values, ranging from 5° to 86° . The number of quasi-perpendicular shocks ($\Theta_{Bn} > 45^\circ$) is slightly higher than the number of quasi-parallel shocks ($\Theta_{Bn} \leq 45^\circ$), accounting for 52% and 48% of the total, respectively. The mean shock angle at 0.72 au is about 45° (with a median of 47°), which is smaller than the average value observed at 1 au (62° – 64°) reported by previous studies (Bavassano-Cattaneo et al. 1986;

Berdichevsky et al. 2000; Lario et al. 2005; Neugebauer 2013; Kilpua et al. 2015; Oliveira & Raeder 2015). All studies mentioned above found that there are more quasi-perpendicular than quasi-parallel IP shocks at 1 au. Oliveira & Raeder (2015) noted that 76% of fast forward IP shocks have $\Theta_{Bn} > 45^\circ$, while Lario et al. (2005) reported the median Θ_{Bn} value is 65° near the orbit of Earth. Thus the shock angle seems to be more perpendicular at 1 au. Similar results were obtained by Volkmer & Neubauer (1985), who found that quasi-parallel shocks occur more frequently between 0.3 and 1 au. This discrepancy is probably related to the form of the Parker spiral. The average IMF is along the Parker spiral and its orientation becomes more tangential when it goes outward in the heliosphere, $\sim 36^\circ$ at 0.7 au against $\sim 45^\circ$ at 1 au, making shock normal more quasi-perpendicular to the ambient IMF direction with a larger heliocentric distance. This result may

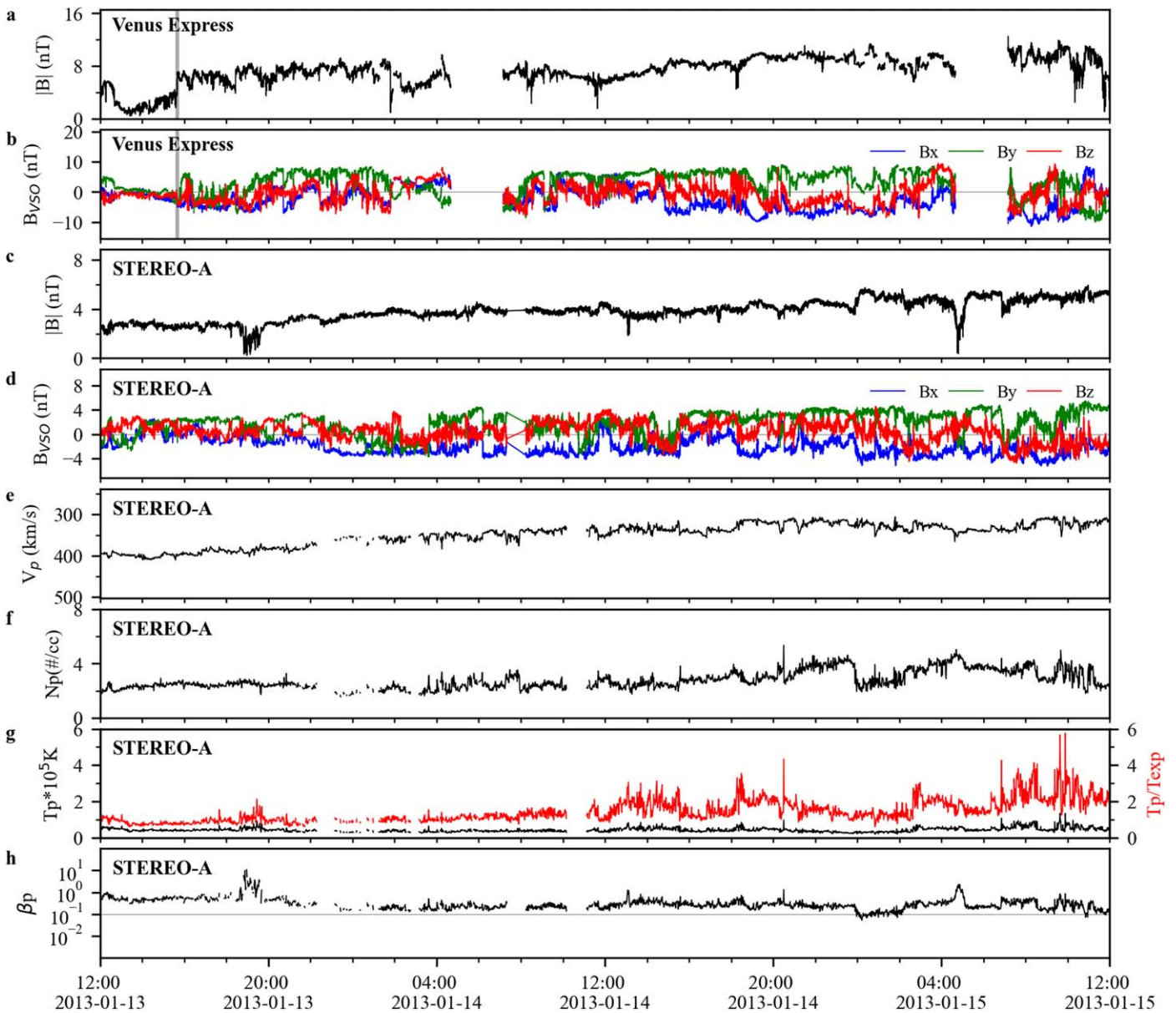


Figure 3. VEX and STEREO-A measurements from 2013 January 13 to 15. The panels from top to bottom represent: (a) the magnetic field strength at VEX; (b) B_x , B_y , B_z magnetic field components at VEX in VSO coordinates; (c) the magnetic field strength at STEREO-A; (d) B_x , B_y , B_z magnetic field components at STEREO-A in VSO coordinates; (e)–(h) the proton bulk speed, the proton density, temperature (red solid line, expected temperature from Lopez 1987), and proton β at STEREO-A. The vertical gray line in (a) and (b) marks the possible fast forward IP shock.

also suggest that the dissipation is more efficient for quasi-parallel shocks at 0.72 au and they are less likely to reach 1 au.

Figure 5(b) shows the shock occurrence versus the magnetic compression ratio. As seen here, the magnetic compression ratio peaks at 2.0–2.25 and most of the shocks, about 65%, have magnetic compression ratios in the range 1.5–2.5. The mean and median values are 2.1 and 2.01 respectively, which are higher than the average shock strength at 1 au. Berdichevsky et al. (2000) have obtained an average magnetic compression ratio of 1.9 based on Wind observations, while Bavassano-Cattaneo et al. (1986) found a mean value of 1.95 at 1 au.

We also note that quasi-perpendicular shocks have, on average, a stronger shock strength than quasi-parallel shocks at 0.72 au. Figure 6 shows that the occurrence of quasi-perpendicular shocks in the range 2.25–4.5 is higher than

quasi-parallel shocks. The mean magnetic compression ratio values are 2.18 for quasi-perpendicular shocks and 2.02 for quasi-parallel shocks.

3.3. Properties of CME-driven Shocks

For the identification of ICME structures at Venus, we referred to two ICME catalogs. The first catalog is from Good & Forsyth (2016), with a total of 84 ICMEs observed by VEX from 2006 to 2013. ICMEs listed in this catalog were identified by magnetic field data alone and by the presence of clear magnetic flux rope signatures. The second catalog comes from Möstl et al. (2017), which updated the Good & Forsyth (2016) database and covered events from 2007 to 2014. With the help of the merged ICME list, we visually inspected all 143 IP shocks and searched for associated ICMEs within 24 hr after the shocks; some new ICMEs that were not previously

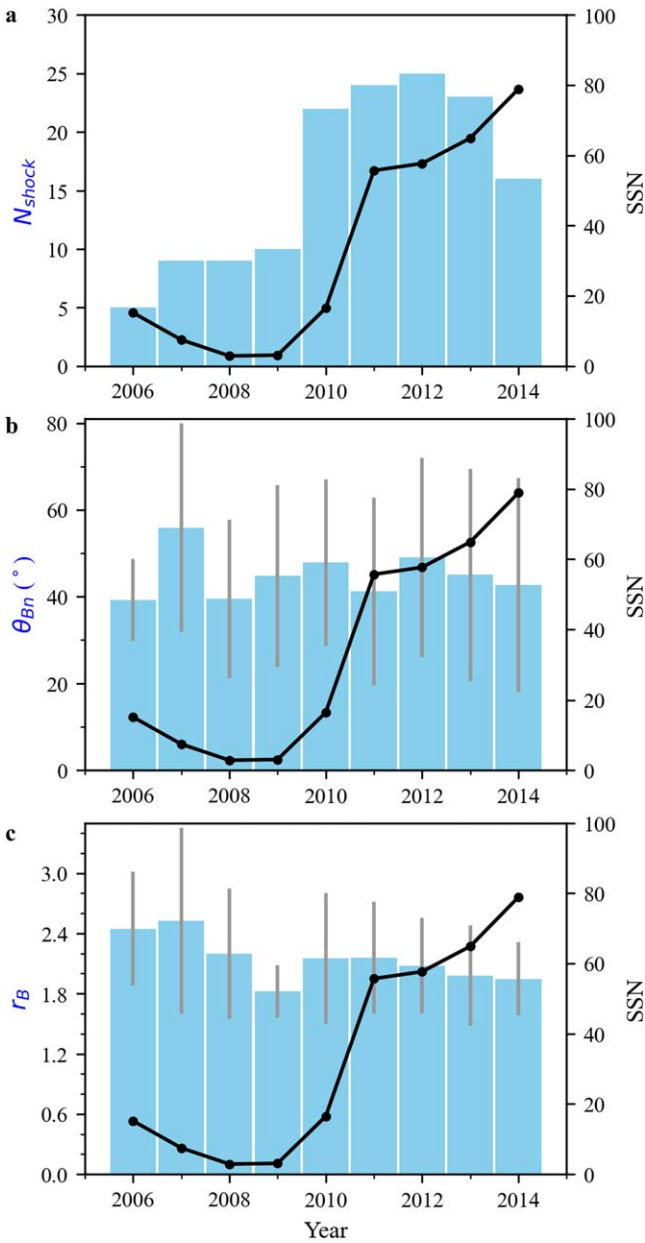


Figure 4. Solar cycle variations of fast forward IP shocks observed at 0.72 au. The histograms of (a) the annual number of IP shocks (N_{shock}), (b) the annual mean of the shock angle (θ_{Bn}), and (c) the annual mean of the magnetic compression ratio (r_B). In each panel, the solid black line represents the annual mean number of sunspots (SSN) and the error bars represent the standard deviations.

identified were detected and added to the list. The final ICME list contains 109 ICMEs during the whole period of VEX observations. IP shocks can be divided into two categories based on the presence or absence of detected ICMEs. We find 58 IP shocks associated with detected ICMEs in our shock list, and 85 remaining shocks have no detected ICME behind them, as shown by the last column in Table 1.

Based on the identifications, we found that about half of ICMEs have leading fast forward IP shocks and 52% of ICMEs drive shocks, which is consistent with the previous finding obtained using PVO data reported by Jian et al. (2008). The ratio of ICMEs driving shocks is slightly lower at 0.72 au than at 1 au; Chi et al. (2016) and Wu & Lepping (2016) suggested that 61% and 58% of ICMEs have leading shocks, respectively.

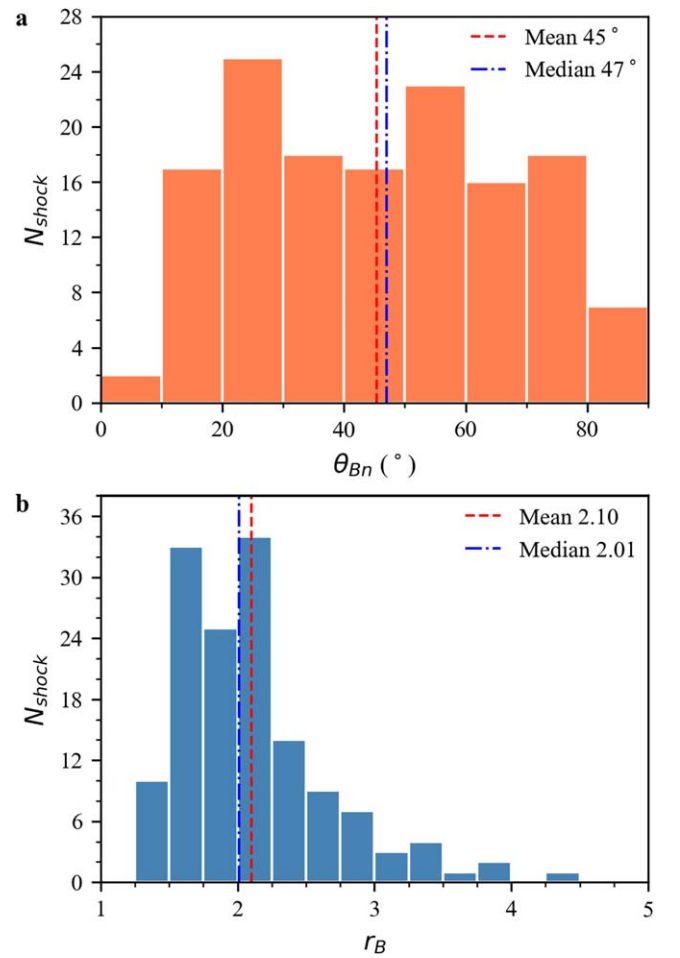


Figure 5. Distribution of shock parameters for fast forward IP shocks observed at 0.72 au. The panels are (a) the shock angle (θ_{Bn}) and (b) the magnetic compression ratio (r_B). In each plot, the red dashed line marks the mean value, and the blue dashed-dotted line marks the median value for all investigated events.

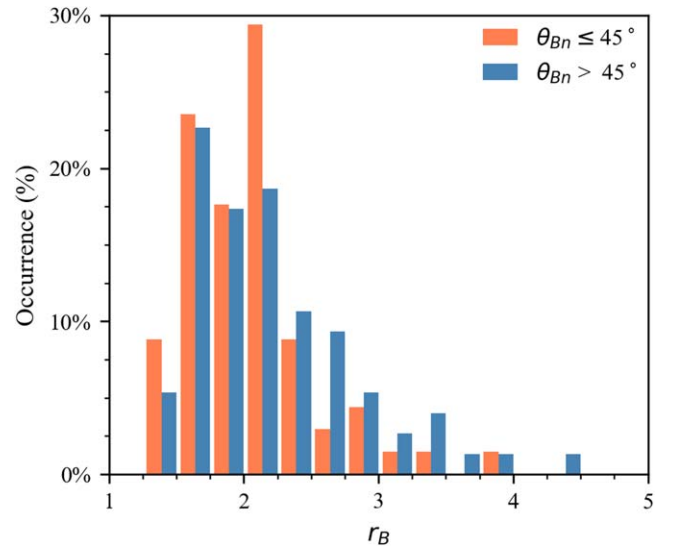


Figure 6. Distribution of the magnetic compression ratio (r_B) for quasi-perpendicular shocks and quasi-parallel shocks. The orange bars represent the magnetic compression ratio for quasi-parallel shocks, and the blue bars represent the magnetic compression ratio for quasi-perpendicular shocks.

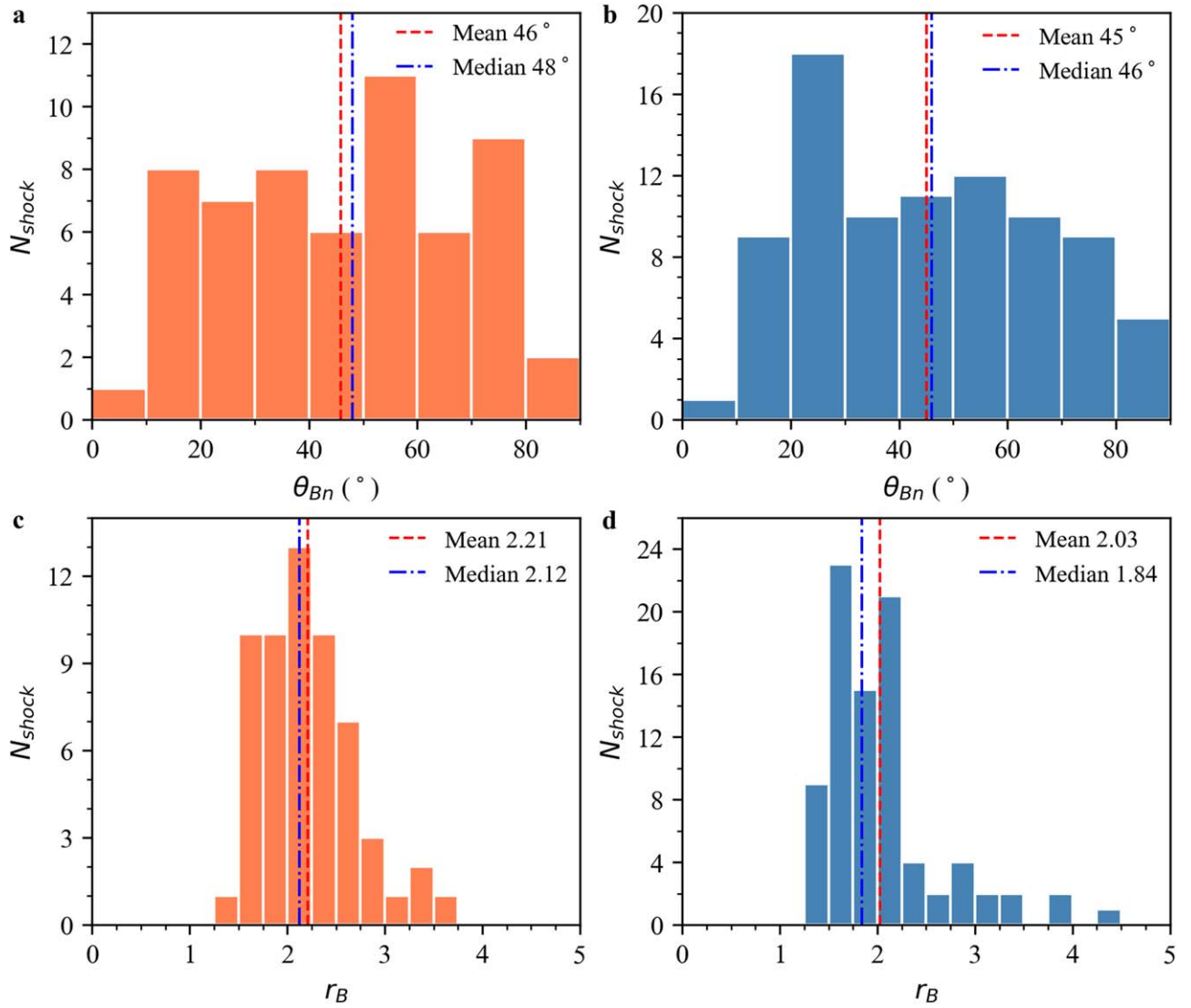


Figure 7. Distribution of shock parameters for fast forward IP shocks with and without a detected ICME driver. (a), (c) The shock angle (Θ_{Bn}) and magnetic compression ratio (r_B) for shocks associated with an observed ICME. (b), (d) The shock angle (Θ_{Bn}) and magnetic compression ratio (r_B) for IP shocks without a detected ICME structure. In each plot, the red dashed line marks the mean value, and the blue dashed-dotted line marks the median value.

We also found that during the whole 2006–2014 period, out of the 143 fast forward IP shocks in our shock list, 58 (41%) of them are associated with observed ICME signatures, while at 1 au, most of the IP shocks (60%) are driven by ICMEs (Oh et al. 2007). Besides, Lindsay et al. (1994) found that most IP shocks (80%) detected by PVO at 0.7 au are associated with ICMEs, which is higher than our finding. This discrepancy may originate from various criteria for shocks and ICMEs in different studies, especially considering that Venus has only magnetic field observations.

Further we investigate the characteristics of IP shocks with an ICME detected by VEX. As shown in Figure 7, for fast forward shocks with and without detected ICME signatures, their mean values of the shock angle are 46° and 45° , with standard deviations of 22° and 21° . The mean values of the magnetic compression ratio are 2.21 and 2.03, with standard deviations of 0.48 and 0.60, respectively. In general, there is no significant difference in shock intensity and shock angle between shocks with and without an associated detected ICME. This result indicates that the shocks without a detected ICME mentioned in this paper are more likely to be driven by

ICMEs. Because ICMEs are smaller in longitudinal extent than shocks, some ICME-driven shocks exist whose driving ICMEs are missed by the observation. Another possibility is that actually these shocks are not driven by ICMEs. In many previous statistical studies about ICME-driven shocks at 1 au, the median values of the shock angle and magnetic compression ratio are about 65° and 2.0 (Lario et al. 2005; Kilpua et al. 2015; Chi et al. 2016), while in our study, those two values are 48° and 2.12, respectively. This indicates that shocks associated with a detected ICME have, on average, a stronger shock strength and smaller shock angle at 0.72 au than at 1 au, which is similar to the result obtained from all IP shock events, and could be accounted for by the IMF spiral and dissipation as explained above.

4. Summary and Conclusion

The measurements by VEX provide an opportunity to further study the properties of IP shocks at 0.72 au. In this paper, we investigated VEX magnetic field data to look for fast forward IP shocks and calculate their shock parameters. We performed

a statistical analysis of solar cycle variations and properties of IP shocks. The major results found in this paper are listed below:

- (1) A shock list covering the time period from 2006–2014 is compiled, which includes 143 fast forward IP shock candidates observed by VEX at 0.72 au.
- (2) The yearly occurrence of IP shocks shows a clear variation with the number of sunspots, and the maximum number of shocks was found in 2012. However, the shock strength and the shock angle do not vary with solar cycle. The magnetic compression ratio is slightly weaker at the solar maximum, which may be caused by the enhanced IMF of background upstream solar wind at the solar maximum, as suggested by Oh et al. (2007).
- (3) Statistical results derived from the present study show that more than half of the events (52%) are quasi-perpendicular shocks, with an average shock angle of 45° . The average shock strength, characterized by the average magnetic compression ratio, is 2.1 at 0.72 au, and quasi-perpendicular shocks have on average stronger shock strength than quasi-parallel shocks. A comparison to other results at 1 au suggests that, on average, fast forward IP shocks are stronger and less perpendicular near Venus than near Earth.
- (4) In general, IP shocks with and without an associated detected ICME show no significant differences in terms of shock intensity and shock angle. Furthermore, similar to our above results, shocks associated with detected ICMEs are generally stronger and less perpendicular at 0.72 au than at 1 au.

For investigating shock properties, it is also important to consider the associated uncertainties in shock parameters. The shock normal is the greatest source of error in our study; in general, the magnetic coplanarity theorem is not always accurate in determining the orientation of IP shocks (Taylor 1969; Viñas & Scudder 1986). The primary problem in estimating an accurate shock normal comes from the sensitive dependence on fluctuations or discontinuities in magnetic field (Esparza & Balogh 2001). The magnetic coplanarity method is sensitive to short term fluctuations in IMF, and errors in the upstream and downstream magnetic field can cause large errors in the shock normal. The second source of uncertainty is the magnetic coplanarity method itself which fails for perpendicular ($\Theta_{\text{Bn}} = 90^\circ$) or parallel ($\Theta_{\text{Bn}} = 0^\circ$) shocks, and the uncertainty in the shock normal becomes large for nearly perpendicular/parallel shocks (Viñas & Scudder 1986; Esparza & Balogh 2001). This is a consequence of the upstream and downstream magnetic fields being approximately parallel or equal to each other, generating significant uncertainty in their cross product, and therefore in the shock normal and the shock angle Θ_{Bn} . The limitations of the coplanarity theorem have been noted by several authors; the statistical analysis by Horbury et al. (2002) showed that the shock normal determined using the coplanarity method is believed to be accurate to 10° – 20° for $\Theta_{\text{Bn}} < 70^\circ$. Tsurutani & Lin (1985) compared Θ_{Bn} obtained using the magnetic coplanarity theorem with those obtained using the mixed-mode technique (Abraham-Shrauner 1972), they found that the shock normal angle of forward shocks is accurate to about 12° . Therefore, although the typical uncertainties for the shock normal are of the order of 10° – 20° , the uncertainties are unlikely to affect our conclusions above.

As discussed in our study, IP shock properties evolve as they propagate away from the Sun. So far, most knowledge about IP shocks is derived from statistical studies based on single-spacecraft observation. Measurements made by a single spacecraft provide some information about local shock properties, while IP shock evolution is still not completely understood, due to the lack of suitable multipoint observations. Our new catalog of IP shocks near Venus is particularly useful for further IP shock evolution studies. By linking individual events observed at VEX to observations at other different heliocentric distance, e.g., Mercury Surface, Space Environment, Geochemistry, and Ranging (MESSENGER), Wind, ACE, STEREO, Tianwen-1, and Mars Atmosphere and Volatile Evolution (MAVEN), we are able to track the same IP shock and obtain a continuous picture of IP shock propagation in IP space. Multipoint observations at different locations can allow us to examine the radial variations of IP shock properties, and to understand the governing physics behind IP shock propagation in the heliosphere. In the future, we plan to investigate the radial evolution of IP shocks with the help of multipoint observations.

We acknowledge the Venus Express team for providing the data. We also thank the World Data Center SILSO (<http://www.sidc.be/silso/>) for use of the sunspot number data, as well as the HELCATS consortium for providing catalogs of ICMEs seen by Venus Express. This work is supported by grants from the Strategic Priority Program of CAS (XDB41000000), NSFC (42004143, 41822405, 41774181, 41774178, 41904151), the Fundamental Research Funds for the Central Universities (WK2080000140, WK2080000122), project funded by China Postdoctoral Science Foundation (2019M652194), and Anhui Provincial Natural Science Foundation (1908085MD107).

ORCID iDs

Can Wang  <https://orcid.org/0000-0002-2865-4626>
 Mengjiao Xu  <https://orcid.org/0000-0002-2924-7520>
 Yutian Chi  <https://orcid.org/0000-0001-9315-4487>
 Yuming Wang  <https://orcid.org/0000-0002-8887-3919>

References

- Abraham-Shrauner, B. 1972, *JGR*, **77**, 736
 Abraham-Shrauner, B., & Yun, S. H. 1976, *JGR*, **81**, 2097
 Barabash, S., Sauvaud, J. A., Gunell, H., et al. 2007, *P&SS*, **55**, 1772
 Bavassano-Cattaneo, M. B., Tsurutani, B. T., Smith, E. J., & Lin, R. P. 1986, *JGR*, **91**, 11929
 Berdichevsky, D. B., Szabo, A., Lepping, R. P., Viñas, A. F., & Mariani, F. 2000, *JGR*, **105**, 27289
 Chai, L., Fraenz, M., Wan, W., et al. 2014, *JGRA*, **119**, 9464
 Chi, Y., Shen, C., Wang, Y., et al. 2016, *SoPh*, **291**, 2419
 Colburn, D. S., & Sonett, C. P. 1966, *SSRv*, **5**, 439
 de Lucas, A., Schwenn, R., dal Lago, A., et al. 2011, *JASTP*, **73**, 1281
 Echer, E., & Gonzalez, W. D. 2004, *GeoRL*, **31**, L09808
 Echer, E., Gonzalez, W. D., Guarnieri, F. L., Lago, A. D., & Vieira, L. E. A. 2005, *AdSpR*, **35**, 855
 Echer, E., Gonzalez, W. D., Tsurutani, B. T., & Gonzalez, A. L. C. 2008, *JGRA*, **113**, A05221
 Echer, E., Gonzalez, W. D., Vieira, L. E. A., et al. 2003, *BrJPh*, **33**, 115
 Esparza, J. A. G., & Balogh, A. 2001, *Geofl*, **40**, 53, <http://www.revistas.unam.mx/index.php/geofisica/article/view/39692>
 Fairfield, D. H. 1976, *RvGeo*, **14**, 117
 Gonzalez, W. D., Tsurutani, B. T., & Clúa de Gonzalez, A. L. 1999, *SSRv*, **88**, 529
 Good, S. W., & Forsyth, R. J. 2016, *SoPh*, **291**, 239

- Gosling, J. T., Hundhausen, A. J., & Bame, S. J. 1976, *JGR*, **81**, 2111
- Horbury, T. S., Cargill, P. J., Lucek, E. A., et al. 2002, *JGRA*, **107**, 1208
- Huttunen, K. E. J., & Koskinen, H. E. J. 2004, *AnGeo*, **22**, 1729
- Jian, L., Russell, C. T., Luhmann, J. G., & Skoug, R. M. 2008, *AdSpR*, **41**, 259
- Kilpua, E. K. J., Balogh, A., von Steiger, R., & Liu, Y. D. 2017, *SSRv*, **212**, 1271
- Kilpua, E. K. J., Lumme, E., Andreeova, K., Isavnin, A., & Koskinen, H. E. J. 2015, *JGRA*, **120**, 4112
- Lario, D., Hu, Q., Ho, G. C., et al. 2005, in ESA Special Publication 592, Proc. Solar Wind 11/SOHO 16 Conf.: Connecting Sun and Heliosphere, ed. H. Lacoste (Noordwijk: ESA), 81
- Lindsay, G. M., Russell, C. T., Luhmann, J. G., & Gazis, P. 1994, *JGR*, **99**, 11
- Lopez, R. E. 1987, *JGR*, **92**, 11189
- Luhmann, J. G. 1986, *SSRv*, **44**, 241
- Mihalov, J. D. 1985, *JGR*, **90**, 210
- Mihalov, J. D., Russell, C. T., Knudsen, W. C., & Scarf, F. L. 1987, *JGR*, **92**, 3385
- Möstl, C., Isavnin, A., Boakes, P. D., et al. 2017, *SpWea*, **15**, 955
- Neugebauer, M. 2013, *SSRv*, **176**, 125
- Oh, S. Y., Yi, Y., & Kim, Y. H. 2007, *SoPh*, **245**, 391
- Oliveira, D. M., & Raeder, J. 2015, *JGRA*, **120**, 4313
- Oliveira, D. M., & Samsonov, A. A. 2018, *AdSpR*, **61**, 1
- Omidi, N. 1995, *RvGeo*, **33**, 629
- Reames, D. V. 1999, *SSRv*, **90**, 413
- Russell, C. T., Chou, E., Luhmann, J. G., et al. 1988, *JGR*, **93**, 5461
- Shan, L., Lu, Q., Mazelle, C., et al. 2015, *P&SS*, **109**, 32
- Shen, C., Xu, M., Wang, Y., Chi, Y., & Luo, B. 2018, *ApJ*, **861**, 28
- Smith, E. J., & Wolfe, J. H. 1976, *GeoRL*, **3**, 137
- Svedhem, H., Titov, D. V., McCoy, D., et al. 2007, *P&SS*, **55**, 1636
- Taylor, H. E. 1969, *SoPh*, **6**, 320
- Titov, D. V., Svedhem, H., Koschny, D., et al. 2006, *P&SS*, **54**, 1279
- Tsurutani, B. T., & Lin, R. P. 1985, *JGR*, **90**, 1
- Vech, D., Stenberg, G., Nilsson, H., et al. 2016, *JGRA*, **121**, 3951
- Viñas, A. F., & Scudder, J. D. 1986, *JGR*, **91**, 39
- Volkmer, P. M., & Neubauer, F. M. 1985, *AnGeo*, **3**, 1
- Wu, C. C., & Lepping, R. P. 2016, *SoPh*, **291**, 265
- Xiao, S. D., Zhang, T. L., Voros, Z., et al. 2020, *JGRA*, **125**, e27190
- Zhang, T. L., Baumjohann, W., Delva, M., et al. 2006, *P&SS*, **54**, 1336
- Zhang, T. L., Baumjohann, W., Du, J., et al. 2010, *GeoRL*, **37**, L14202
- Zhang, T. L., Baumjohann, W., Russell, C. T., Luhmann, J. G., & Xiao, S. D. 2016, *NatSR*, **6**, 23537
- Zhang, T. L., Delva, M., Baumjohann, W., et al. 2008, *P&SS*, **56**, 790
- Zhang, T. L., Du, J., Ma, Y. J., et al. 2009, *GeoRL*, **36**, L20203
- Zurbuchen, T. H., & Richardson, I. G. 2006, *SSRv*, **123**, 31